AD-A187 464 TACTILE SENSING AND INVERSE PROBLEMS(U) MARYLAND UNIV 1/1
COLLEGE PARK R YANG ET AL OCT 87 AFOSR-TR-87-1435
AFOSR-87-0073

UNCLASSIFIED F/G 12/9 NL

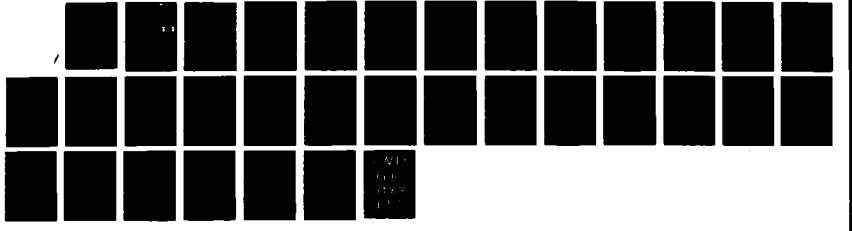

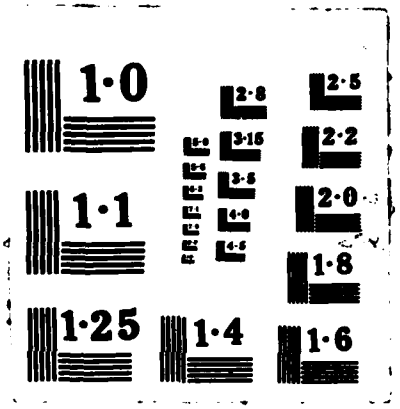
1·0
1·1
1·25
1·4
1·6
1·8
2·0
2·2
2·5
2·8
3·15
3·5
4·0
4·5

Tactile Sensing and Inverse Problems[1]

R. Yang and P. S. Krishnaprasad

Department of Electrical Engineering

and

Systems Research Center

University of Maryland

College Park, Maryland 20742

oct 1987

1. Introduction

In recognizing a grasped object or grasp an object stably with a multifingered robotic hand, tactile sensors mounted on robot fingers have been identified as essential detecting tool. In general, grasp stability has two requirements: sliding avoidance and excess force avoidance. Hence, it is required that a tactile sensor be able to detect the nature of the force distribution which exists between the surface of the grasped object and the robot finger.

Recently, much work has been devoted to the tactile sensing problem. Several kinds of the tactile sensors have been designed based on electro-optics, piezoresistive, or piezoelectric properties,etc.. Typically, these sensors are not used to measure the contact force directly, but to measure the interior strain or stress in an elastic finger pad. When sharp and rigid objects, e.g. a wedge indentor, indent an elastic

[1]This work was supported in part by the National Science Foundation under grant OIR-85-00108 and AFOSR-URI grant AFOSR-87-0073.

1a. REPORT SECURITY CLASSIFICATION		1b. RESTRICTIVE MARKINGS	
2a. SECURITY CLASSIFICATION AUTHORITY		3. DISTRIBUTION/AVAILABILITY OF REPORT approved for public release; distribution unlimited.	
2b. DECLASSIFICATION/DOWNGRADING SCHEDULE			
4. PERFORMING ORGANIZATION REPORT NUMBER(S)		5. MONITORING ORGANIZATION REPORT NUMBER(S) AFOSR-TR- 87-1435	
6a. NAME OF PERFORMING ORGANIZATION	6b. OFFICE SYMBOL (*If applicable*)	7a. NAME OF MONITORING ORGANIZATION	
6c. ADDRESS (*City, State, and ZIP Code*)		7b. ADDRESS (*City, State, and ZIP Code*)	
8a. NAME OF FUNDING/SPONSORING ORGANIZATION	8b. OFFICE SYMBOL (*If applicable*)	9. PROCUREMENT INSTRUMENT IDENTIFICATION NUMBER AFOSR-87-0073	
8c. ADDRESS (*City, State, and ZIP Code*)		10. SOURCE OF FUNDING NUMBERS	
		PROGRAM ELEMENT NO.	PROJECT NO. / TASK NO. / WORK UNIT ACCESSION NO.
11. TITLE (*Include Security Classification*)			
12. PERSONAL AUTHOR(S)			
13a. TYPE OF REPORT	13b. TIME COVERED FROM _____ TO _____	14. DATE OF REPORT (*Year, Month, Day*) Oct. 1987	15. PAGE COUNT
16. SUPPLEMENTARY NOTATION			

17. COSATI CODES			18. SUBJECT TERMS (*Continue on reverse if necessary and identify by block number*)
FIELD	GROUP	SUB-GROUP	

19. ABSTRACT (*Continue on reverse if necessary and identify by block number*)

20. DISTRIBUTION/AVAILABILITY OF ABSTRACT ☐ UNCLASSIFIED/UNLIMITED ☐ SAME AS RPT. ☐ DTIC USERS	21. ABSTRACT SECURITY CLASSIFICATION	
22a. NAME OF RESPONSIBLE INDIVIDUAL	22b. TELEPHONE (*Include Area Code*)	22c. OFFICE SYMBOL

material, very high stress is developed at the contact surface. This stress is reduced by distance from the contact area, so a fragile sensor would be better protected within a layer soft material. Another advantage of using an elastic covering is that the contact area becomes large so that grasp stability may be enhanced and the features of grasped objects better distinguished.

The goal of this paper is to study how a surface force profile may be estimated from the information on strain or stress distribution detected by tactile sensors. This problem is referred to as the inverse problem since we can consider the stress or strain within an elastic material as the response due to surface loading. This inverse problem can be treated as a deconvolution problem or, more generally, as the problem of solving an operator equation of the first kind. It is of interest to determine how such an ill-posed problem may be solved using appropriate regularization(Tikhonov 1977). In this paper, we will not consider the effects of the noises (or suppose the observations have been passed through some kind of filter) and only pay attention to deriving particular operators, analyzing their properties and using the Discrete Fourier Transform(DFT) approach to solve the associated equations.

In Section 2, we will study a particular model of the elastic material, i.e. the relation between the surface load and stress or strain beneath the surface. In Section 3, we will investigate an approximate method to solve the inverse problem for some special cases. In Section 4, we will give some examples and compare the results.

We are collaborating closely with a research group at the Naval Research Laboratory under Dr. M. Peckerer, involved in the fabrication of silicon-based tactile sensor. We are also comparing our numerical results against analog network solutions to the inverse problem of this paper.

2. The model of the elastic material

In this section, we attempt to find the relation between the load profile, which exists on the surface of a half space of elastic material, and the distribution of the stress or the strain beneath the surface of that material. To specify the load, we shall just consider the contact force profile rather than the contact displacement profile for the following reasons:

- The contact stress is more directly useful for stable grasping.
- There is a complex relation between displacement profile and surface stress profile.(Phillips and Johnson, 1981)

In this paper, the elastic characteristics of the material are assumed to be homogeneous and isotropic. In addition, the dimension of the contact area will be assumed to be infinitely large in a direction, say z, such as a line load. By that assumption, we just need to analyze two dimensional behavior in a slice perpendicular to that direction.

From the theory of elasticity(Timoshenko and Goodier, 1951), under above assumptions about the material, the differential equation of the equilibrium and the boundary condition for the stress are linear. Consequently, it is possible to consider the interior stress or strain distribution due to a general contact as the superposition of those quantities due to a set of line contacts.

We now study the behavior of an infinite homogeneous and isotropic elastic material under line contact with negligible contact width. For a two dimensional problem in polar coordinates, the distribution of stress follows a simple radial distribution. From the theory of elasticity(Timoshenko and Goodier, 1951), for the concentrated force inclined from the vertical by an angle, $\alpha < \pi/2$, we have

$$\sigma_r = \frac{2F\cos(\theta - \alpha)}{\pi r}$$

$$\sigma_\theta = 0$$

$$\tau_{r\theta} = 0$$

where σ_r is the radial stress at the point (r, θ), σ_θ is the stress in the plane at (r, θ) normal to the radial stress, $\tau_{r\theta}$ is the shearing stress in the r, θ-plane, F is the force per unit length and r is the distance from the point of application. Note that we have defined the normal stress to be positive when it produces compression. Fig.1. shows the above variables.

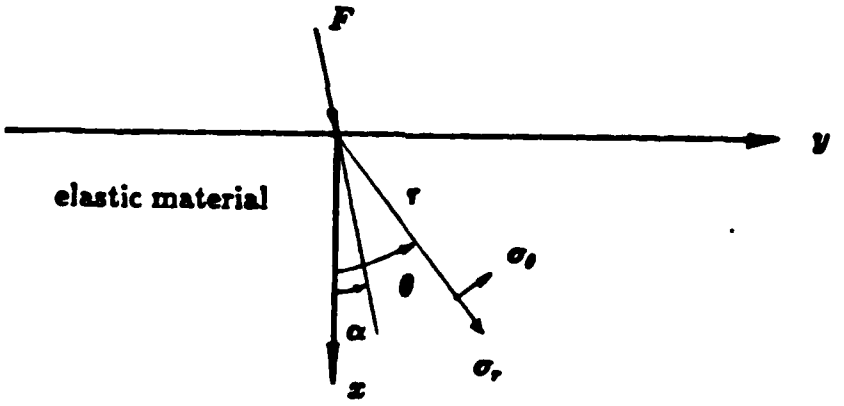

Fig. 1. Line force on elastic half-plane

Applying the tensor transformation

$$\sigma_x = \sigma_r \cos^2\theta$$

$$\sigma_y = \sigma_r \sin^2\theta$$

we get the stress expression in Cartesian coordinates

$$\sigma_x = \frac{2F}{\pi r} cos(\alpha - \theta) cos^2\theta \tag{1}$$

$$\sigma_y = \frac{2F}{\pi r} cos(\alpha - \theta) sin^2\theta$$

where $r = \sqrt{x^2 + y^2}$, $cos\theta = x/r$, $sin\theta = y/r$. By decomposing F into vertical component, F_v , and tangential component, F_t , we have

$$sin\alpha = \frac{F_t}{F} \tag{2}$$

$$cos\alpha = \frac{F_v}{F}$$

Then Eq.(1) can be expressed as

$$\sigma_x = \frac{2x^2}{\pi(x^2 + y^2)^2}(xF_v + yF_t) \tag{3}$$

$$\sigma_y = \frac{2y^2}{\pi(x^2 + y^2)^2}(xF_v + yF_t)$$

We will only consider σ_x since, in y direction, it converges faster than σ_y as $y \to \pm\infty$. Applying the principle of superposition, we have, for a load distributed along the y-axis,

$$\sigma_x(x,y) = \int_{-\infty}^{\infty} [K_1^{stress}(x, y - y_0)F_v(y_0) + K_2^{stress}(x, y - y_0)F_t(y_0)]dy_0 \tag{4}$$

where

$$K_1^{stress}(x,y) = \frac{2x^3}{\pi(x^2 + y^2)^2}$$

$$K_2^{stress}(x,y) = \frac{2x^2y}{\pi(x^2+y^2)^2}$$

for $y \in \mathrm{R}$ and $x \in (0,\infty)$. $F_v(y)$ and $F_i(y)$ are the surface stress distributions in x and y direction, respectively. Fig. 2. shows the $K_1^{stress}(x,y)$ and $K_2^{stress}(x,y)$ for $x = 1$ and $x = 2$.

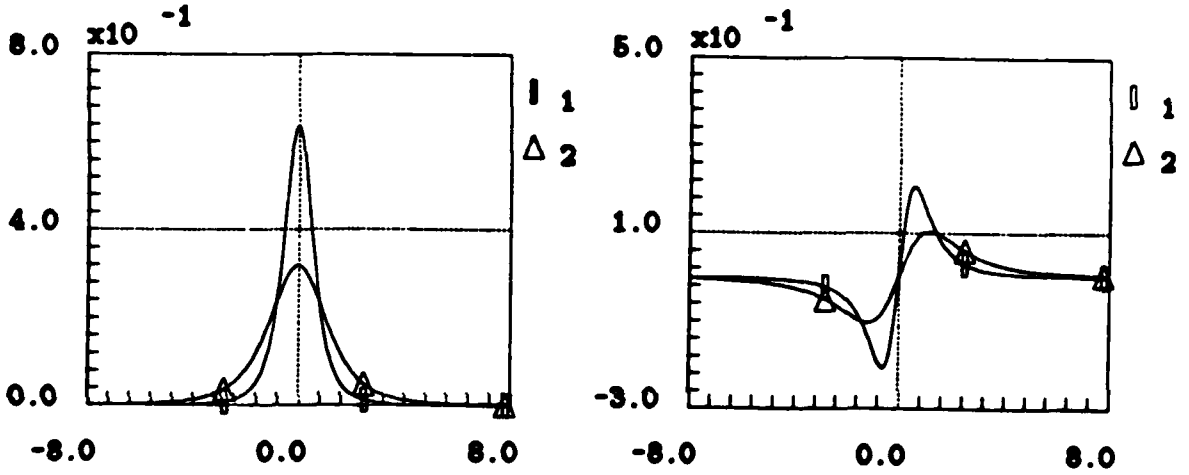

Fig. 2. Functions of K_1^{stress} and K_2^{stress} at $x = 1$ and $x = 2$

Since many pressure sensors have outputs based on the strain of the sensor , which is the fractional change in the linear dimensions of a small cubic volume element, e.g. electric-resistance strain gauges, we need to find the relations between the components of stresses and the components of the strains. By Hooke's Law in the theory of elasticity, we have

$$\epsilon_x = \frac{1}{E}[\sigma_x - \nu(\sigma_y + \sigma_z)]$$

$$\epsilon_y = \frac{1}{E}[\sigma_y - \nu(\sigma_x + \sigma_z)] \qquad (5)$$

$$\epsilon_z = \frac{1}{E}[\sigma_z - \nu(\sigma_x + \sigma_y)]$$

where E is the modulus of elasticity, ν is Poisson's ratio, ϵ_x ϵ_y and ϵ_z are the components of strains along x, y, z direction , respectively.

Using the plane strain assumption which states that for a line force of infinite extension on an elastic half-space, the strain in the direction of the line, ϵ_x, must be zero by symmetry. Then Eq.(5) becomes

$$\epsilon_x = \frac{1}{E}[(1-\nu^2)\sigma_x - \nu(\nu+1)\sigma_y] \tag{6}$$

$$\epsilon_y = \frac{1}{E}[(1-\nu^2)\sigma_y - \nu(\nu+1)\sigma_x]$$

From Eq(6), we can get the expression of σ_x by ϵ_x and ϵ_y

$$\sigma_x = \lambda[(1-\nu)\epsilon_x + \nu_y\epsilon_y] \tag{7}$$

where

$$\lambda = \frac{E}{(1+\nu)(1-2\nu)}$$

It should be note that if ν=0.5, from Eq.(6), $\epsilon_x = -\epsilon_y = \frac{3}{4E}(\sigma_x - \sigma_y)$. That means there is not enough information from ϵ_x and ϵ_y to determine σ_x or σ_y . In this paper, when we use the strain distribution in x direction as the only sensed data to solve the inverse problem, we always assume that ν is 0.5. Actually, the Poisson's ratio of rubberlike materials, which usually are used to cover robot fingers and tactile sensors, is 0.5 approximately.

We will see in the end of section 4, the surface force profile reconstructed from stress distribution is more accurate than from strain distribution after they are truncated.

Again, using the principle of superposition for general contact, we have

$$\epsilon_z(x,y) = \int_{-\infty}^{\infty} [K_1^{strain}(x, y-y_0)F_v(y_0) + K_2^{strain}(x, y-y_0)F_t(y_0)]dy_0 \qquad (8)$$

where

$$K_1^{strain}(x,y) = \frac{3x(x^2-y^2)}{2\pi E(x^2+y^2)^2}$$

$$K_2^{strain}(x,y) = \frac{3y(x^2-y^2)}{2\pi E(x^2+y^2)^2}$$

for $y \in \mathrm{R}$ and $x \in (0,\infty)$. Fig. 3. shows the $K_1^{strain}(x,y)$ and $K_2^{strain}(x,y)$ for $x=1$ and $x=2$.

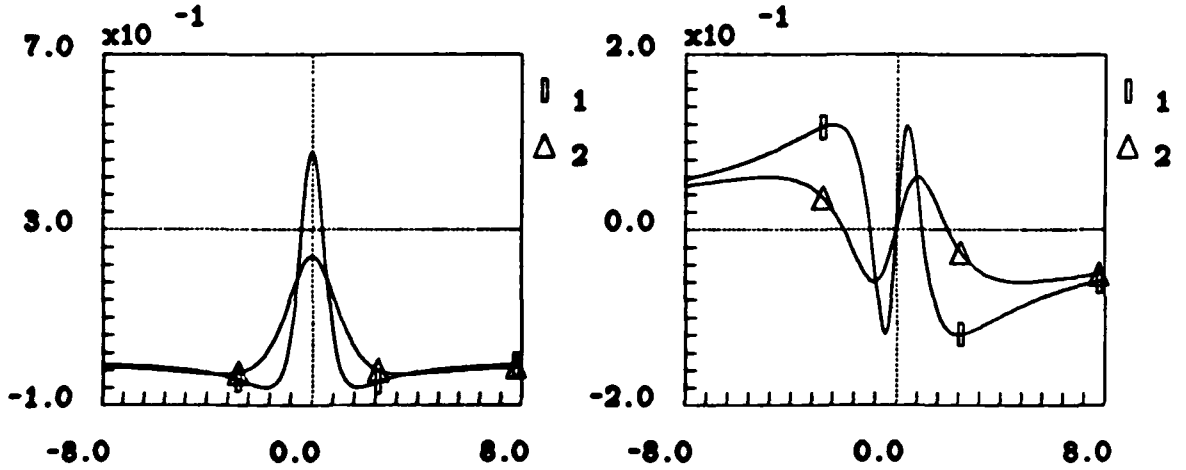

Fig. 3. Functions of K_1^{strain} and K_2^{strain} at $x=1$ and $x=2$.

In sake of convenience, we write Eq.(4) and Eq.(8) in the general form as

$$g(y) = \int_{-\infty}^{\infty} [K_1(y-y_0)F_v(y_0) + K_2(y-y_0)F_t(y_0)]dy_0 \qquad (9)$$

where $y \in R$. We will indicate that K_1, K_2 and g are in the form of stress or strain when it is necessary. In Eq.(9), there is no x dependence since we assume that the array of tactile sensors is usually mounted on a horizontal plane beneath the surface of elastic material. Thus, x in Eq.(9) is a constant which expresses the depth of the sensors from the surface.

3. The DFT approach for inverse problem

In this section, a method to solve Eq.(9) approximately will be examined. We will assume that $F_v(y)$ is produced by the strip contact, i.e. it satisfies

$$F_v(y) = \begin{cases} F_1(y), & \text{if } y \in [a_1, a_2]; \\ 0, & \text{otherwise,} \end{cases}$$

where $F_1(y)$ is a continuous function defined on $[a_1, a_2]$, $F_1(y) > 0$ for $y \in (a_1, a_2)$ and $F_1(y) \geq 0$ at $y = a_1$ and $y = a_2$, for some finite a_1 and a_2. Moreover, we will assume that $\mid a_i \mid < A/2$, $i = 1, 2$, where A is the half width of surface of the finger. We made this assumption because, even for a very narrow force profile, a broad distribution of stress and strain will be produced . This can be illustrated by Fig.2 and Fig.3 which show the distribution of stress and strain due to line contact when we let one of F_v and F_t be unit impulse function and another be zero. In other words, for a strip contact, we need the observations which distribute more broadly than the width of the strip to obtain the surface force profile. About $F_t(y)$, we will just consider two special cases which may happen during the grasping process. In addition, we will assume that the modulus of elasticity, E, is one in the rest of this paper.

3.1 Surface force profile without tangential component

This situation may happen when a robot hand grasps an object , which lies on a stable support, to determine if the normal force is large enough to lift the object. In this case, Eq.(9) becomes

$$g(y) = \int_{-\infty}^{\infty} K_1(y - y_0) F_v(y_0) dy_0 \qquad y \in R \tag{10}$$

This integral equation is of convolution type, in which $g(y)$ is the observation obtained by sensors, $F_v(y)$ is an unknown function, $K_1(y)$ is usually called the kernel.

Mathematically, to recover the unknown function, $F_v(y)$, from the data of $g(y)$ is referred to as the deconvolution problem or, in general, the problem of solving operator equation of the first kind. This problem is ill-posed in the sense of Hadamard (1923). Several methods for this problem have been derived which all try to find a solution by supplementing the calculations with some extra information, for example, generalized inverse and regularization, etc.(Hilgers, 1973).

Next, we will examine a method depending on the Fourier Transform. It is known that the Fourier Transform of the convolution of K_1 and F_v equals to the normal multiplication of Fourier Transform of K_1 and F_v if

$$\int_{-\infty}^{\infty} \mid K_1(y) \mid dy < \infty$$

and

$$\int_{-\infty}^{\infty} \mid F_v(y) \mid dy < \infty$$

That is,

$$\hat{K}_1(\omega)\hat{F}_v(\omega) = \hat{g}(\omega) \tag{11}$$

where $\hat{K}_1(\omega), \hat{F}_v(\omega)$ and $\hat{g}(\omega)$ are Fourier Transforms of K_1, F_v and g, respectively. It is clear that if $\hat{K}_1(\omega) \neq 0$, $\forall|\omega| < \infty$ and $\hat{g}(\omega)/\hat{K}_1(\omega) \in L_1(-\infty, \infty)$, the Eq.(10) can be solved simply as

$$F_v(y) = \mathcal{F}^{-1}(\frac{\hat{g}(\omega)}{\hat{K}_1(\omega)}) \qquad y \in R \tag{12}$$

Actually, it is easy to check that, for K_1^{stress} and K_1^{strain} given in Eq.(4) and Eq.(8), their Fourier Transforms are

$$\hat{K}_1^{stress}(\omega) = e^{-x|\omega|}(1 + x|\omega|) \quad \omega \in R$$

and

$$\hat{K}_1^{strain}(\omega) = 1.5x|\omega|e^{-x|\omega|} \quad \omega \in R$$

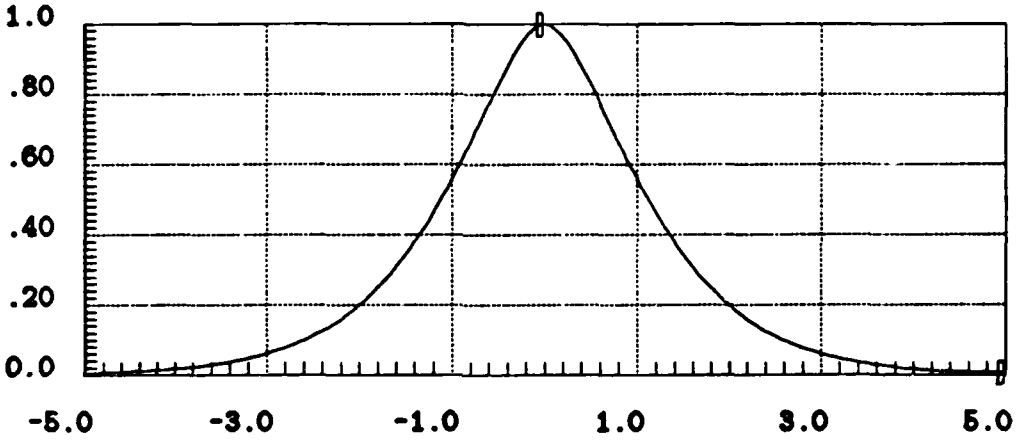

Fig. 4. The Fourier Transform of K_1^{stress} at $x = 1.5$.

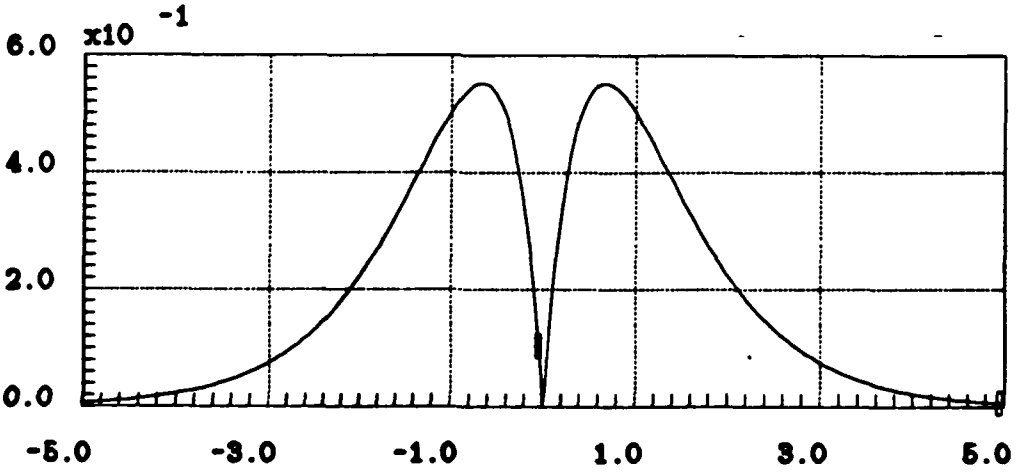

Fig. 5. The Fourier Transform of K_1^{strain} at $x = 1.5$.

From Fig.4., we find that if the distribution of stress can be obtained directly or indirectly by sensors, the inverse problem can be solved by Eq.(12). If we have to use the distribution of strain, the conditions of Eq.(12) can no be satisfied since $\hat{K}_1^{strain}(0) = 0$, (see Fig.5). We will see later that this problem will be solved when the observation, $g(y)$, is truncated and DFT is applied.

Physically, the continuous expression of $g(y)$ can not be obtained directly, but only the discrete data of $g(y)$. So, we are forced to apply the Discrete Fourier Transform to solve the inverse problem approximately.

The discretization of Eq. (10) is

$$g(y_n) = \sum_{i=-\infty}^{\infty} K_1(y_n - y_i) F_v(y_i) \Delta y_i \qquad n = 0, \pm 1, \pm 2, \ldots \tag{13}$$

where $\Delta y_i = y_{i+1} - y_i$. If we let Δy_i be identical for all i, denoted by Δ, which will be called the sampling period, and denote $g(y_n)$ by $g(n)$, $K_1(y_n - y_i)\Delta y_i$ by $K_1(n-i)$ and $F_v(y_i)$ by $F_v(i)$, then Eq.(13) can be written as

$$g(n) = \sum_{i=-\infty}^{\infty} K_1(n-i) F_v(i) \qquad n = 0, \pm 1, \pm 2, \ldots \tag{14}$$

This is the discrete convolution equation. As we have mentioned before, physically, it is impossible to get the data of observation, $g(n)$, everywhere. We have to cut off $g(n)$, at $n = -N$ and N,where $N\Delta = A$. Due to the properties of $K_1^{stress}(y)$ and $K_1^{strain}(y)$ and the assumption about $F_v(y)$, if A is large enough, $g(N)$ should be very small. Then, we can approximate Eq.(14) as

$$g(n) = \sum_{i=-N}^{N} K_1(n-i) F_v(i) \qquad n = 0, \pm 1, \pm 2, \ldots, \pm N \tag{15}$$

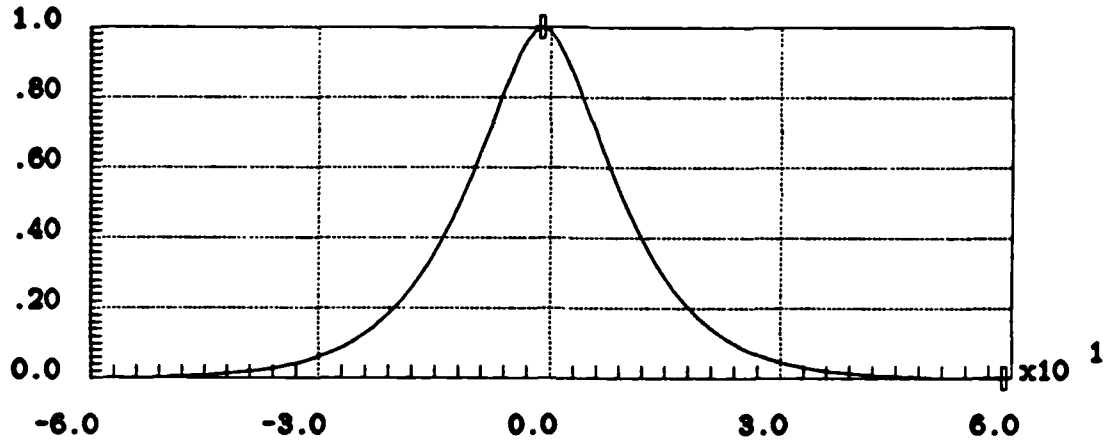

Fig.6 The DFT of K_1^{stress}

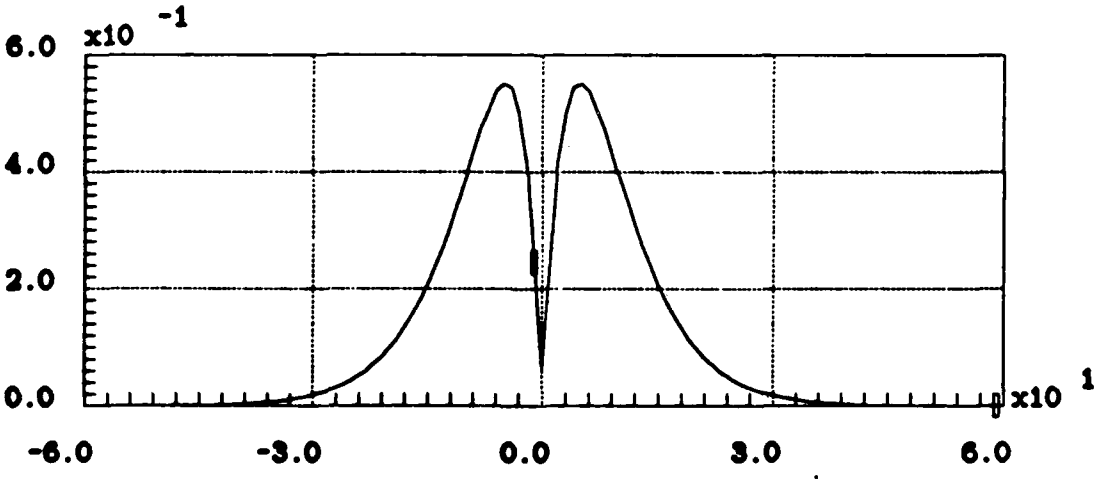

Fig.7 The DFT of K_1^{strain}

It is well known that the discrete Fourier transform of convolution of $K_1(i)$ and $F_v(i)$ is the normal multiplication of DFT of them. So, we have

$$\hat{g}(k) = \hat{K}_1(k)\hat{F}_v(k) \qquad k = 0, \pm 1, \pm 2, ..., \pm N \tag{16}$$

where $\hat{g}(k) = \sum_{i=-N}^{N} g(i)e^{-j2\pi ik/2N+1}$, $j = \sqrt{-1}$, $k = 0, \pm 1, \ldots, \pm N$ is the DFT of $g(i)$, and similar to $\hat{K}_1(k)$ and $\hat{F}_v(k)$. Fig.6 and Fig.7 give the DFT of K_1^{stress} and K_1^{strain}.

From the theory of digital signal processing (Chen,1979), we know that ,if the Fourier Transform of a function is almost zero when $|\omega|$ is greater than the half of the sampling frequency, $2\pi/\Delta$, it will be equal to the discrete Fourier Transform of that function times sampling period at $\omega = 2k\pi/((2N+1)\Delta)$ for $k = 0, \pm 1, \pm 2, ..., \pm N$, where Δ is the sampling period. Comparing Fig.4 and Fig.5 with Fig.6 and Fig.7, we find $K_1^{stress}(y)$ and $K_1^{strain}(y)$ are almost satisfied above condition and result. But, for K_1^{strain}, they are different at 0. The reason is that our function is not periodic and N can not be arbitrary large, i.e. it have to be truncated. This just give us a chance to apply the DFT to solve the inverse problem.

Applying Inverse Discrete Fourier Transform, the unknown function, $F_v(k)$, is

$$F_v(k) = \frac{1}{2N+1} \sum_{r=-N}^{N} \left(\frac{\hat{g}(r)}{\hat{K}_1(r)}\right) e^{j2\pi rk/2N+1} \qquad k = 0, \pm 1, \ldots \pm N \tag{17}$$

In next section, by example, we will find that the reconstructed function produced by Eq.(17) is very accurate with respect to the designed one. We will also discuss the effect of truncation and the choice of K_1.

3.2 Surface force profile with constant tangential component

This situation may happen when a robot hand lifts an object which has a rectangular surface. In order to avoid slipping during grasping, we are interested in

the tangential force on the average, instead of at every point. So, we assume that

$$F_t(y) = \begin{cases} c, & \text{if } y \in [a_1, a_2]; \\ 0, & \text{otherwise,} \end{cases}$$

where c is a constant, and the relation of $F_t(y)$ and $F_v(y)$ at the boundary of cone of friction is estimated by

$$\int_{-\infty}^{\infty} F_t(y)dy = \mu \int_{-\infty}^{\infty} F_v(y)dy.$$

By assumption of F_t,

$$c = \frac{\mu}{a_2 - a_1} \int_{a_1}^{a_2} F_v(y)dy \tag{18}$$

where μ is the coefficient of static friction. Moreover, we assume that $a \stackrel{\text{def}}{=} a_1 = a_2$ since we will need to determine the boundary of the load from $g(y)$. Under above assumptions, Eq.(9) becomes

$$g(y) = \int_{-\infty}^{\infty} [K_1(y - y_0)F_v(y_0) + \frac{\mu}{2a} K_2(y - y_0) \int_{-\infty}^{\infty} F_v(u)du]dy_0 \tag{19}$$

Next, we will discuss how to solve Eq.(19) numerically.

By discretizing Eq.(19) and truncating the observation, we have

$$g(n) = \sum_{i=-N}^{N} K_1(n - i)F_v(i) + \frac{\mu}{2M}(\sum_{i=-N}^{N} u(i)K_2(n - i))(\sum_{k=-N}^{N} F_v(k))$$

$$n = 0, \pm 1, \ldots, \pm N \tag{20}$$

in which M is taken such that $2a = 2M\Delta$, and $u(i)$ is defined as

$$u(i) = \begin{cases} 1, & \text{for } i : i\Delta \in [-a, a]; \\ 0, & \text{otherwise.} \end{cases}$$

Applying DFT to Eq.(20), we have

$$\sum_{n=-N}^{N} g(n)w^{nr} = (\sum_{n=-N}^{N} K_1(n)w^{nr})(\sum_{n=-N}^{N} F_v(n)w^{nr})$$

$$+\frac{\mu}{2M}(\sum_{n=-N}^{N} F_v(n))(\sum_{n=-N}^{N} K_2(n)w^{nr})(\sum_{n=-N}^{N} u(n)w^{nr})$$

$$r = 0, \pm 1, ..., \pm N$$

where $w = e^{-j2\pi/2N+1}, j = \sqrt{-1}$. When $r = 0$,

$$\sum_{n=N}^{N} g(n) = (\sum_{n=-N}^{N} K_1(n))(\sum_{n=-N}^{N} F_v(n)) + \frac{\mu(2M+1)}{2M}(\sum_{n=-N}^{N} K_2(n))(\sum_{n=-N}^{N} F_v(n)) \tag{21}$$

Since $K_2(y)$ is a odd function, we have

$$\sum_{n=-N}^{N} K_2(n) = 0$$

Therefore, Eq.(21) becomes

$$F \stackrel{\text{def}}{=} \sum_{n=-N}^{N} F_v(n) = (\sum_{n=-N}^{N} g(n))(\sum_{n=-N}^{N} K_1(n))^{-1}$$

Discretizing Eq.(18), we have

$$c = \frac{\mu}{2M}F \tag{22}$$

Return to Eq.(20), we have

$$g(n) - c\sum_{i=-M}^{M} K_2(n-i) = \sum_{i=-N}^{N} K_1(n-i)F_v(i) \qquad n = 0, \pm 1, ..., \pm N \tag{23}$$

Denoting left hand side of above equation as $G(n)$, Eq.(23) becomes

$$G(n) = \sum_{i=-N}^{N} K_1(n-i)F_v(i) \qquad n = 0, \pm 1, ... \pm N \tag{24}$$

This is the equation we have solved in above subsection. However, the problem of this subsection has not solved since we do not know M yet. As we have assumed before, $F_v(y)$ and $F_i(y)$ have symmetric support, $[-a, a]$. And we will see in next section that the algorithm in subsection 3.1 has a very good accuracy. By these properties, we can find M. The method is shown as follows.

We have known that

$$g(y) = \int_{-\infty}^{\infty} K_1(y - y_0)F_v(y_0) + K_2(y - y_0)F_i(y_0)dy_0$$

Then,

$$g(-y) = \int_{-\infty}^{\infty} K_1(-y - y_0)F_v(y_0) + K_2(-y - y_0)F_i(y_0)dy_0$$

By changing the integral variable and utilizing the odd and even property of $K_1(y)$ and $K_2(y)$, we have

$$g(-y) = \int_{-\infty}^{\infty} K_1(y - y_0)F_v(-y_0) - K_2(y - y_0)F_i(-y_0)dy_0$$

Since we assumed that $F_i(y)$ is a constant, taking the average of $g(y)$ and $g(-y)$, we have

$$\tilde{g}(y) = \int_{-\infty}^{\infty} K_1(y - y_0)\tilde{F}_v(y_0)dy_0 \tag{25}$$

where $\tilde{g}(y) = [g(y) + g(-y)]/2$, $\tilde{F}_v(y) = [F_v(y) + F_v(-y)]/2$.

By the assumption of $F_v(y)$, $\tilde{F}_v(y)$ still have a symmetric support, $[-a, a]$. Therefore, applying the DFT to Eq.(25), we can find M by the algorithm in subsection 3.1.

4. Examples

In this section we will give some examples for some special load profiles and compare the results which are got from the observations expressed as the distribution of stress and distribution of strain when $\nu = 0.5$.

Some parameters are fixed as follows.

- the depth of the sensors, $x = 1.5$
- the sampling period, $\Delta = 0.5$
- the modulus of elasticity, $E = 1$
- the numbers of elements of sensors, $2N + 1 = 121$

We will consider two kinds of rigid load: cylinder and rectangle, as shown in Fig.8.

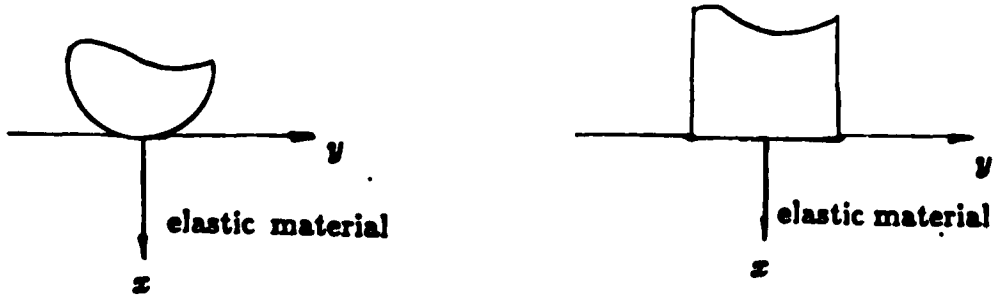

Fig.8 The cylindrical and rectangular indentor

From Conway et al. (1966), for cylinder indenting an elastic half-plane, the surface stress is given by

$$F_v(y) = \begin{cases} \frac{2P}{\pi a^2}\sqrt{a^2 - y^2}, & \text{for } y \in [-a, a]; \\ 0, & \text{otherwise,} \end{cases}$$

where a is the half-width of the contact region and P is the force per length; for rectangular indentor, the stress on the surface is given by

$$F_v(y) = \begin{cases} \frac{P}{\pi\sqrt{a^2 - y^2}}, & \text{for } y \in [-a, a]; \\ 0, & \text{otherwise,} \end{cases}$$

For numerical simulation, we will adjust a by $a + \epsilon$ for $\epsilon \ll 1$, since, physically, $F_v(a)$ can not be infinite large.

In following examples, $g(y)$ is produced by the discrete form of Eq.(4) and Eq.(8) directly. To evaluate the reconstructed surface stress,F_r, with respect to designed one, F, we use the absolute error defined as

$$e = \frac{1}{2N+1}\sum_{i=-N}^{N} |F_r(i) - F(i)|. \tag{26}$$

4.1 Cylinder indenting without friction

The distributions of stress and strain at $x = 1.5$ produced by cylindrical indentor are given in Fig.9 and Fig.11, respectively, in which the designed surface stresses are also displayed. Fig.10 and Fg.12 give the surface stress reconstructed from the observations given in Fig.9 and Fig.11, respectively. For comparing, the designed surface stresses are displayed again.

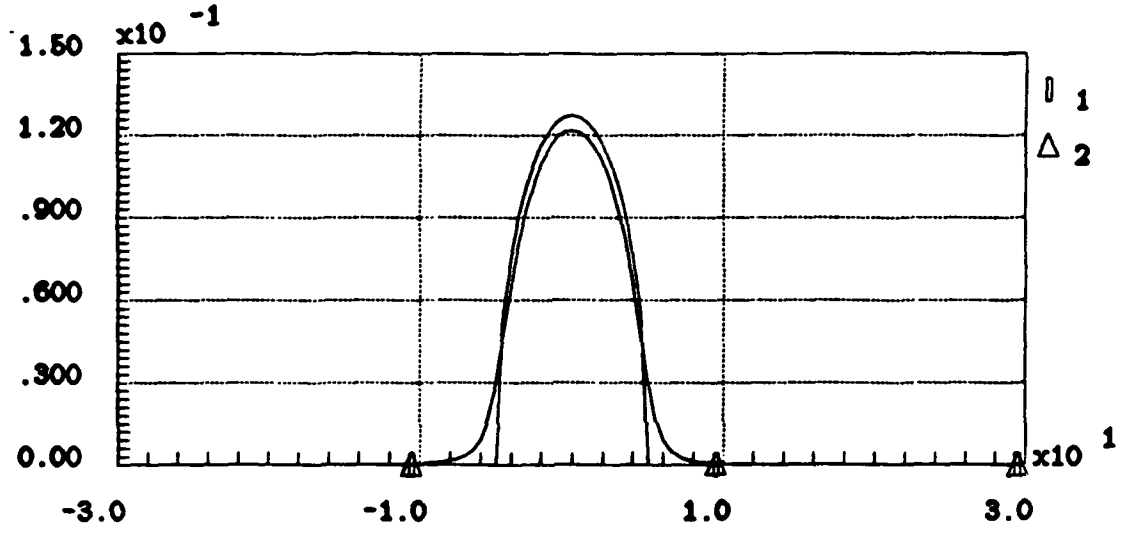

Fig.9 1. the designed surface stress; 2. the stress at $x = 1.5$

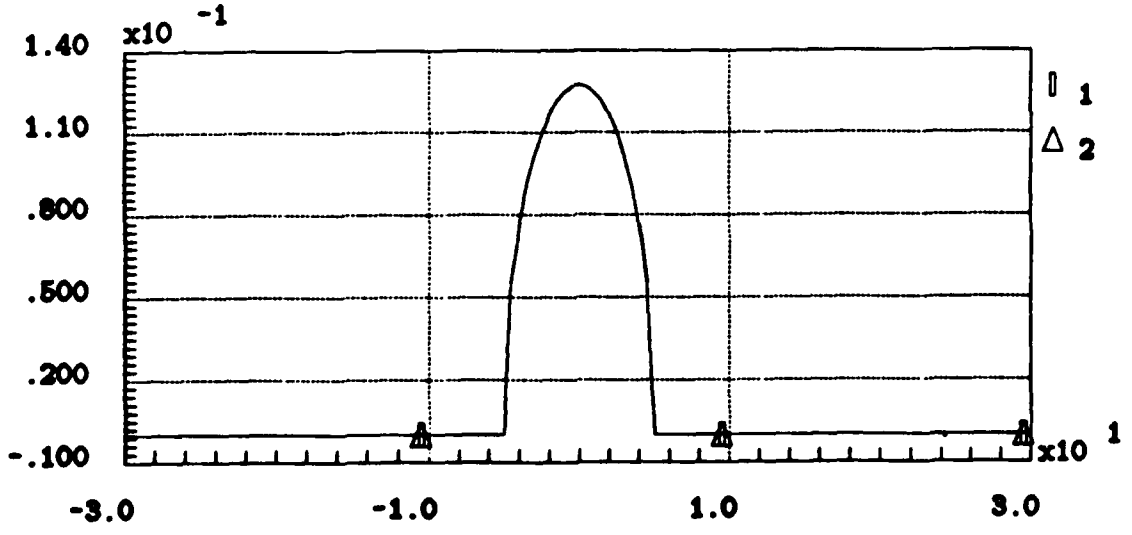

Fig.10 1. the designed surface stress; 2. the reconstructed surface stress

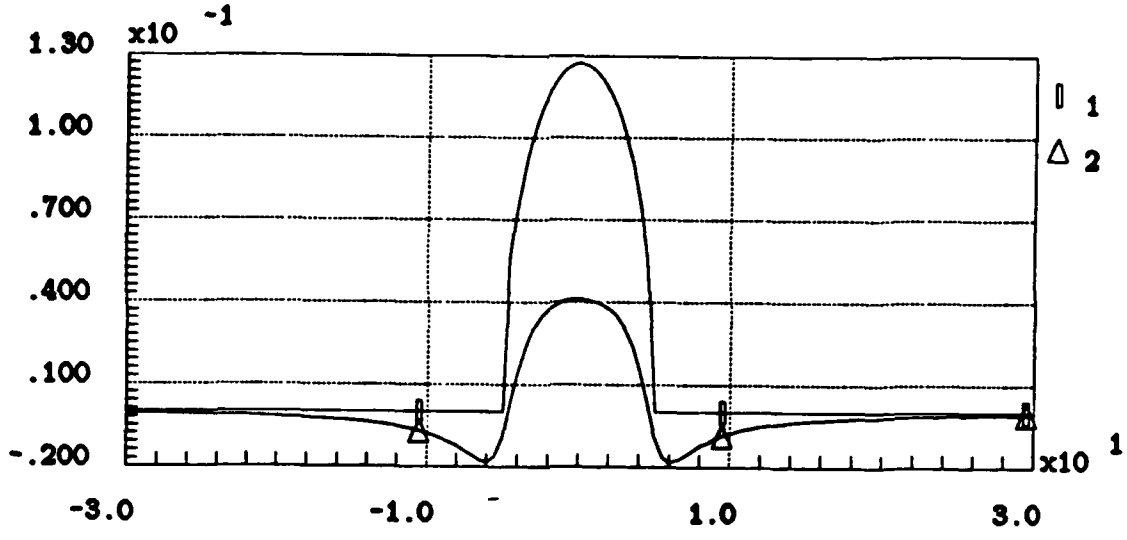

Fig.11 1. the designed surface stress; 2. the strain at $x = 1.5$

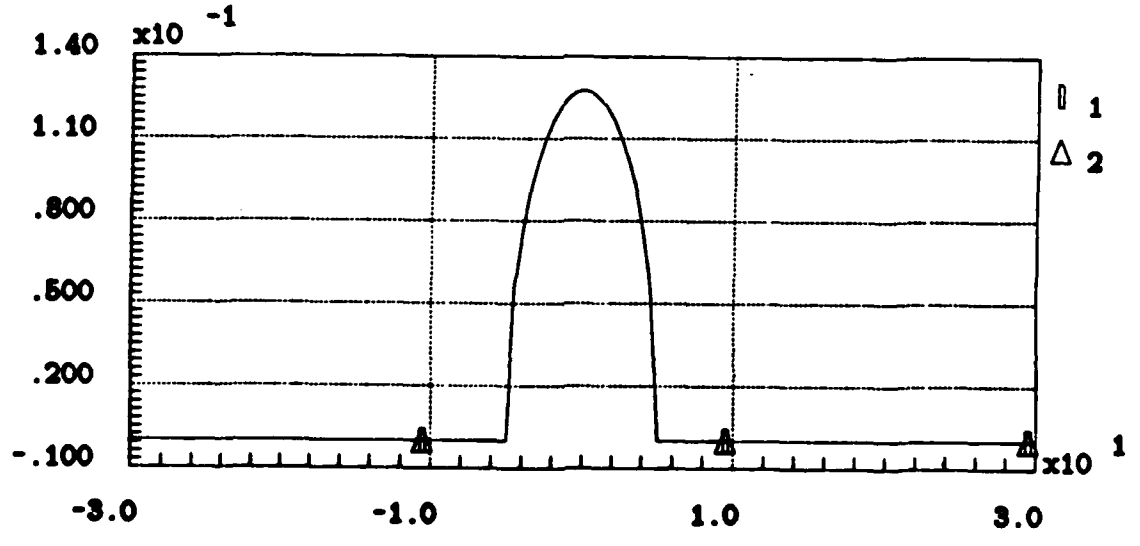

Fig.12 1. the designed surface stress; 2. the reconstructed surface stress

By Eq.(26), the errors for these two cases are

$$e^{stress} = 3.93 \times 10^{-6} \quad , e^{strain} = 4.04 \times 10^{-5}$$

4.2 Rectangle indenting without friction

Fig.13–Fig.16 display the same things given in above subsection for rectangular indenting.

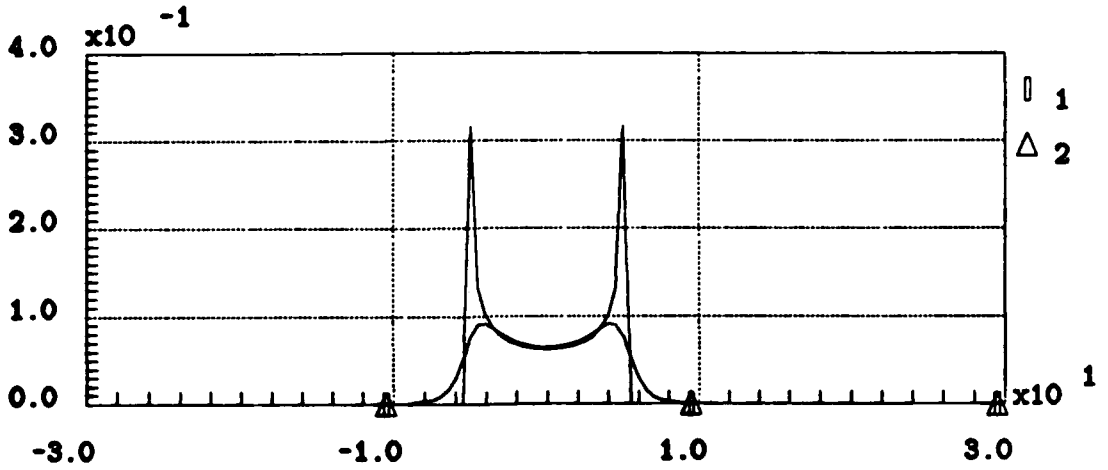

Fig.13 1. the designed surface stress; 2. the stress at $x = 1.5$

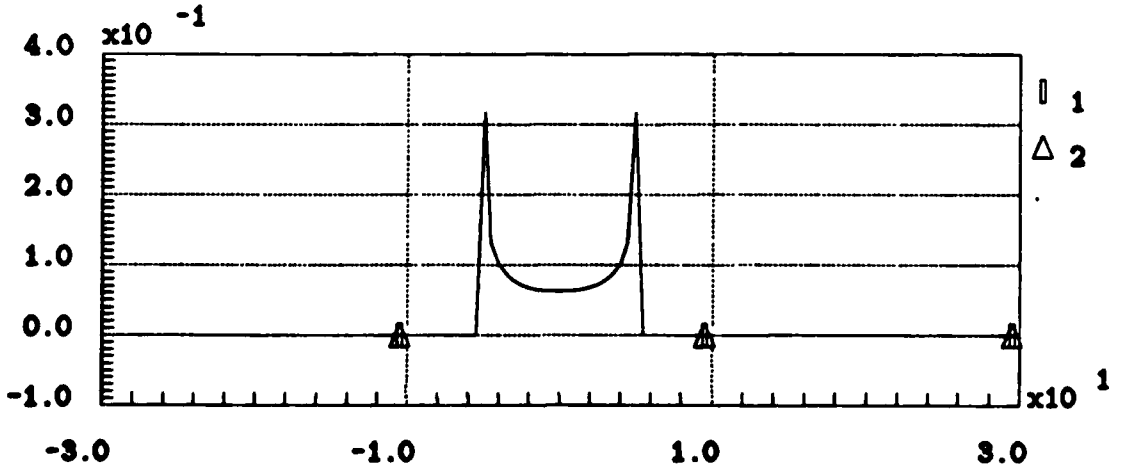

Fig.14 1. the designed surface stress; 2. the reconstructed surface stress

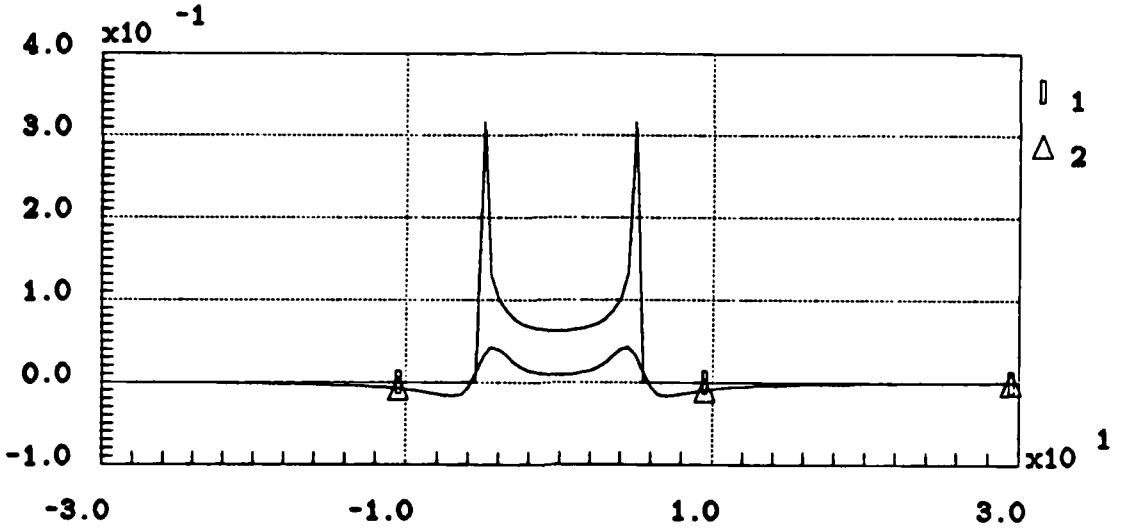

Fig.15 1. the designed surface stress; 2. the strain at $x = 1.5$

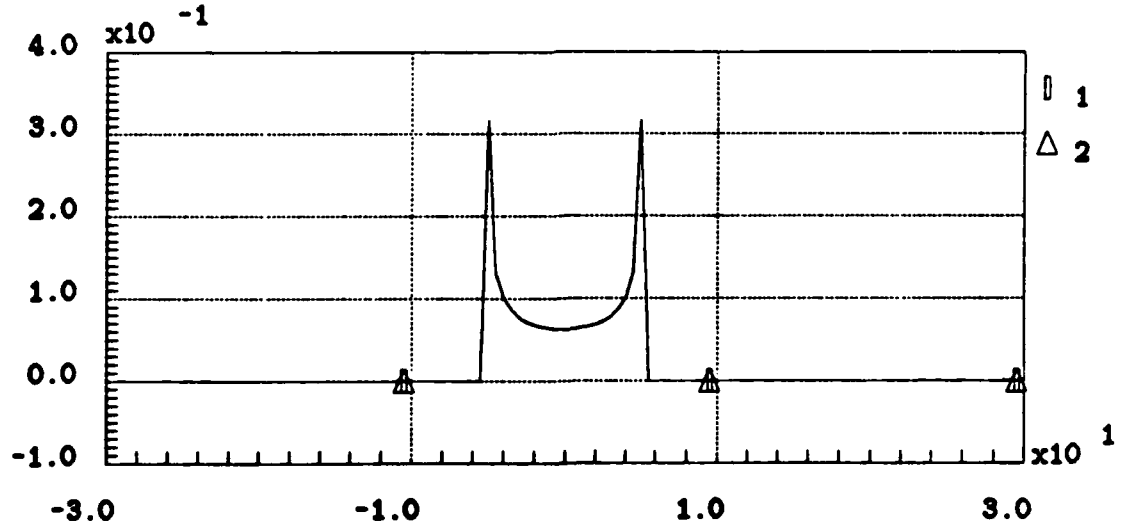

Fig.16 1. the designed surface stress; 2. the reconstructed surface stress

By Eq.(26), the errors for these two cases are

$$e^{stress} = 4.44 \times 10^{-6};\ e^{strain} = 1.06 \times 10^{-4}$$

4.3 Rectangular indenting with constant friction

The distributions of stress and strain at $x = 1.5$ produced by cylindrical indentor are given in Fig.17 and Fig.19, respectively, in which the designed surface stresses in vertical and tangential direction are also displayed. Fig.18 and Fig.20 give the surface stresses reconstructed from the observations given in Fig.17 and Fig.19, respectively. For comparing, the designed surface stresses are displayed again.

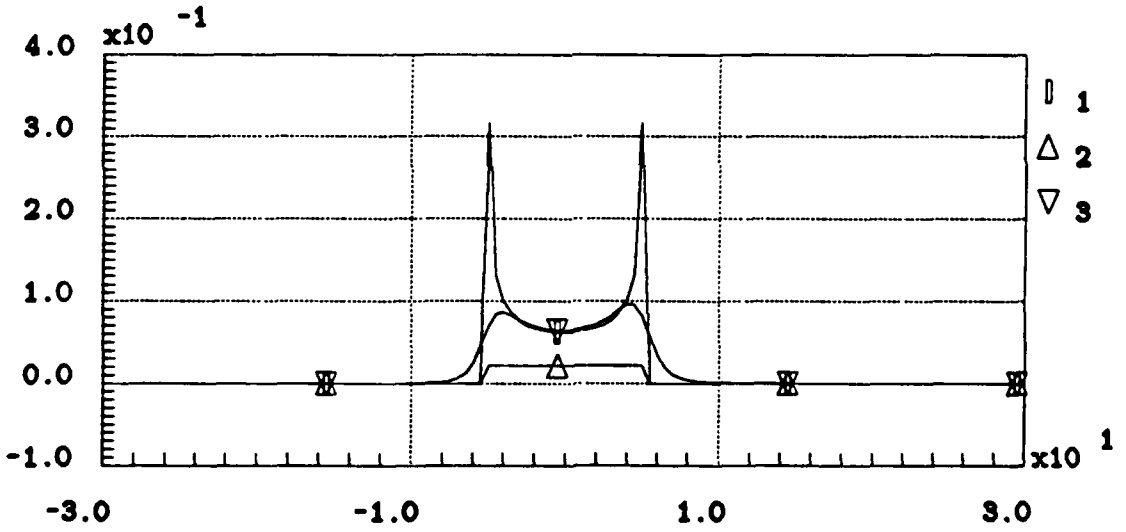

Fig.17 1. the designed vertical surface stress;
2. the designed tangential surface stress;
3. the stress at $x = 1.5$

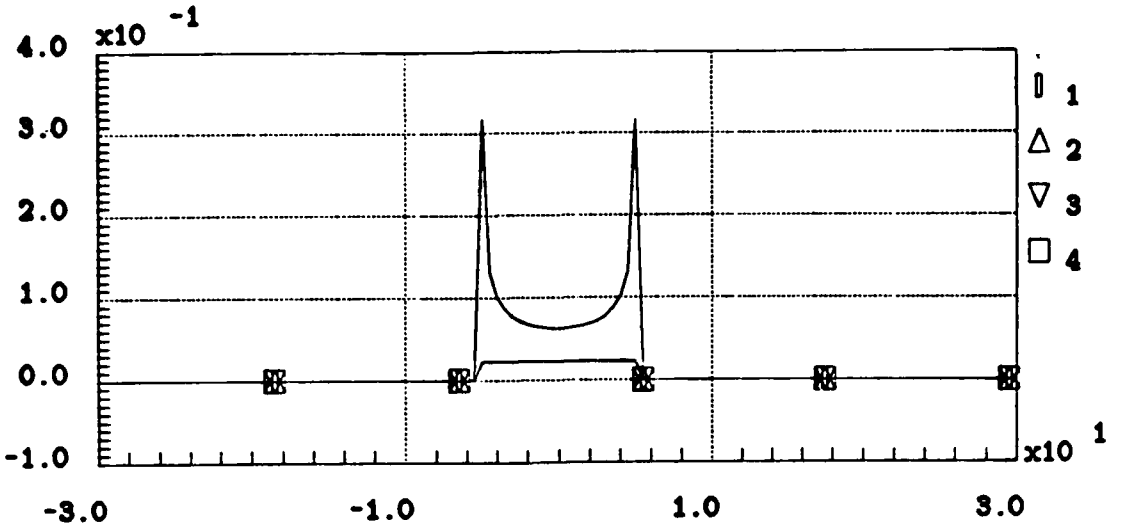

Fig.18 1. the designed vertical surface stress;

2. the reconstructed vertical surface stress

3. the designed tangential surface stress

4. the reconstructed tangential surface stress

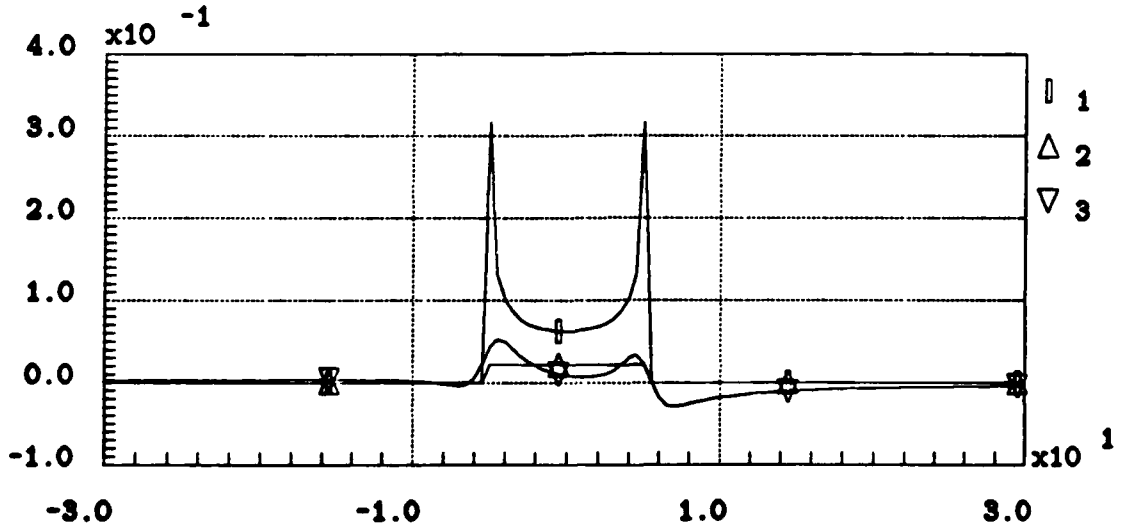

Fig.19 1. the designed vertical surface stress;

2. the designed tangential surface stress; 3. the strain at x =1.5

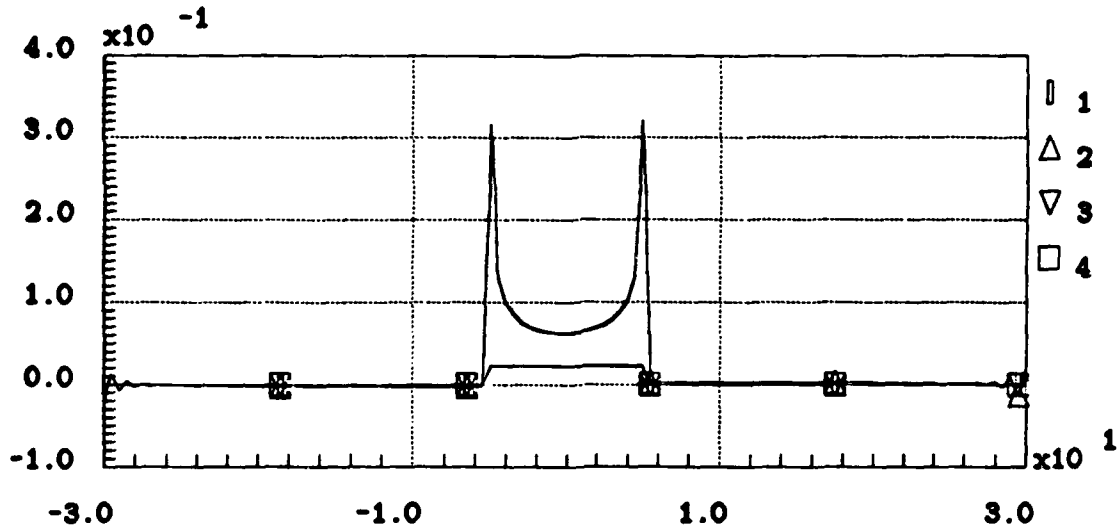

Fig.20 1. the designed vertical surface stress;

2. the reconstructed vertical surface stress
3. the designed tangential surface stress
4. the reconstructed tangential surface stress

By Eq.(26), the errors for these two cases are

$$e_v^{stress} = 6.21 \times 10^{-5}, \quad e_t^{stress} = 1.15 \times 10^{-3}$$

$$e_v^{strain} = 2.95 \times 10^{-3}, \quad e_t^{strain} = 1.45 \times 10^{-3}$$

where the subscripts v and t are expressed for vertical and tangential component, respectively.

From above examples, we find that $e^{strain} > e^{stress}$ for all cases. There are many sources to produce errors. One of them is that the observation has been truncated. We have known that the further the point is from the area of surface load, the little the effect of surface force to strain or stress beneath the surface is. Comparing the distributions of stress and strain for the same load, e.g. Fig.9 and Fig.11, we find

that the effect to the strain is broader than the stress. Thus, more information will be lost when we truncate the observation which is expressed as strain instead of stress. Above argument can be illustrated by Fig.21 and Fig.22, in which the number of element of sensors is only 41.

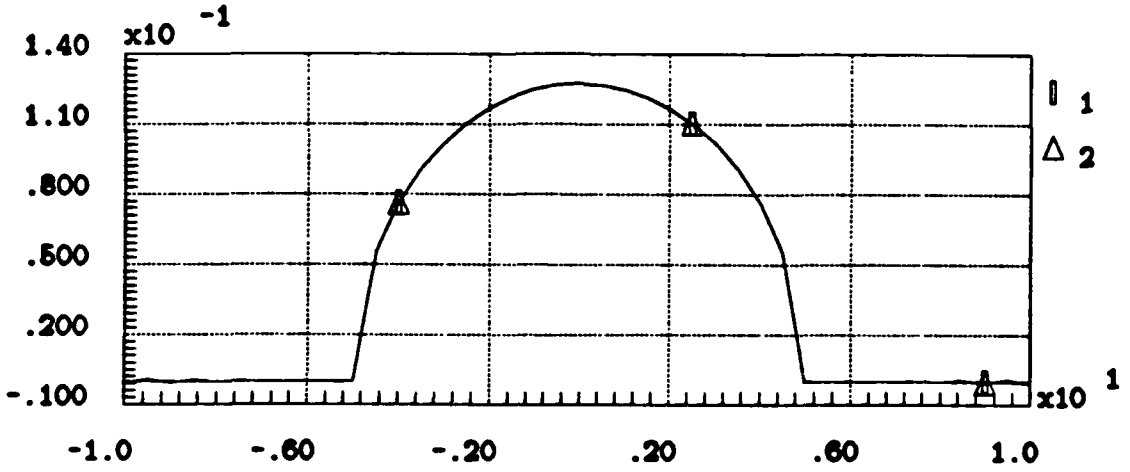

Fig.21 the surface stress reconstructed from the distribution of stress at $x = 1.5$

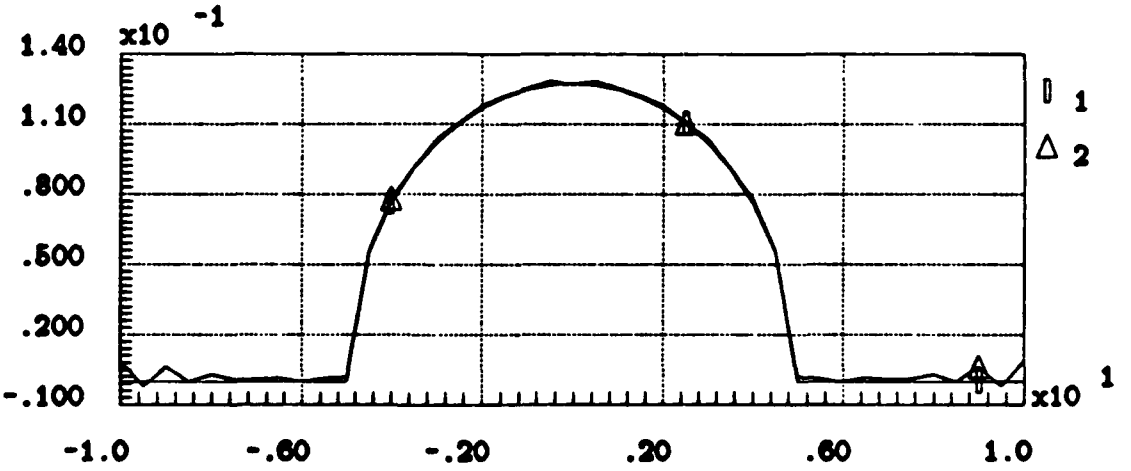

Fig.22 the surface stress reconstructed from the distribution of strain at $x = 1.5$

5. Discussion

In this paper, we described how to express the distribution of stress and strain as the convolution of the surface stress and relative kernel. We gave the DFT approach for two special cases. By example, we discussed the effect of truncation of the observation and the effect of choosing as observation the strain or stress.

As we have mentioned in first section, there are several methods to solve operator equations of first kind. By comparing the DFT approach with one of the regularization methods of Hilgers(1973), we found that the former has the properties of higher computing speed and better accuracy. However, if noise with high frequency is added to the observation, one finds that the DFT method is much more sensitive to the noise, even when the deviation of the noises is very small. It should be noted that, for both of these approaches, the analog networks have been introduced to solve the inverse problem by parallel computation (Poggio,1985; Peckerer). This should be of interest in real time control of the robot fingers.

There are several problems that remain to be solved. One is how to reconstruct the surface stress profile when it has a general tangential distribution. To solve this problem, more information on the strain or the stress is required. Sensors which are mounted on two horizontal planes beneath the surface of elastic material may be helpful for this case. The other problem is how to deal with three dimensional problem, which is important for physical situations. To solve this problem, a more complex model of the elastic material should be applied.

Reference

Chen, C. 1979,

One-dimensional digital signal processing. Marcel Dekker, Inc.

Coway, H. D., et al 1966.

Normal and shearing contact stress in indented strips and slabs.
Int. J. Eng. Sci. 4: 343-359.

Hilgers, J. W. 1973.

Non-iterative methods for solving operator equations of
the first kind. Ph.D thesis, University of Wisconsin-Madsion.

Phillips, J. R. and Johnson, K. O. 1981.

Tactile spatial resolution. III. A continuum mechanics model of skin
predicting mechanoreceptor response to bars, edges, and grating.
J. Neurophys. 46(6):1204-1225.

Poggio, T. , Torre, V. and Koch. C. 1985

Computational vision and regularization theory.
Nature, Vol. 317, No. 6035, pp. 314-319, 26 Sept. 1985

Tikhonov, A. N. and Arsenin, V. Y. 1977

Solutions of Ill-posed Problems
John Wiley and Sons Washington, D.C.

Timoshenko, S., and Goodier, J. N. 1951.

Theory of elasticity. New York: McGraw-Hill

END

FEB.

1988

DTIC